

ARTICLE

Open Access

A three-dimensional in vitro model of the peripheral nervous system

Sunghee Estelle Park^{1,2,3,4}, Jinchul Ahn¹, Hyo-Eun Jeong¹, Inchan Youn^{3,5}, Dongeun Huh^{1,2,4,6} and Seok Chung^{1,7}

Abstract

Recent advances in three-dimensional (3D) cell culture models developed on organ-on-a-chip or microfluidic devices have shown their capability to recapitulate the in vivo microenvironment as well as their potential as tools in biomedical research. Here, we present an in vitro model of the peripheral nervous system (PNS) by establishing a coculture model of motor neurons (MNs) and Schwann cells (SCs) in a 3D environment in a microengineered extracellular matrix hydrogel scaffold. The collagen scaffold placed at the center of the microdevice provided a 3D cellular microenvironment where the axons of MNs were allowed to actively interact with SCs during their growth and maturation. By treating the MN–SC coculture model with ascorbic acid, we were able to model the myelination process in the PNS, which was evidenced by the increased expression of myelin markers in SCs. Moreover, we show that this can be reversed by treating myelinated nerve fibers with glial growth factor (neuregulin-1 isoform) to potentially block the formation of the myelin sheath and induce demyelination. Our 3D cell culture model may be used to achieve active control of the myelinating and demyelinating processes in the PNS and thus may offer new opportunities to study pathophysiological processes involved in motor neuron diseases by in vitro modeling.

Introduction

In the peripheral nervous system (PNS), the continuous bidirectional interaction between axons and Schwann cells (SCs) is important for myelin formation^{1,2}. Axonal signals are responsible for SC migration, proliferation, and differentiation into myelinating or nonmyelinating cells³. Reciprocally, SCs provide trophic support for neuronal maturation, and their signaling induces the sequential assembly of proteins in the process of myelination to organize domains that are essential for efficient action potential propagation⁴. Although the characteristics and potentialities of SCs have been identified, the ability to study axon–SC interactions in a three-dimensional (3D) environment would advance our understanding of physiological

interactions between motor neurons (MNs) and SCs during myelination and demyelination processes.

To better recapitulate physiologically relevant models, it is important that such model systems move beyond traditional cell cultures to models that specifically mimic the physiological and biochemical aspects of organs or tissues. A variety of in vitro myelination models of PNS have been developed to study demyelinating diseases, where pathological processes are expected to mimic human diseases (Supplementary Table 1)^{4,5}. However, they do not allow accurate replication of the PNS since traditional in vitro models are mainly developed in two-dimensional (2D) cell culture settings where neurons are cultured on the surface of a coverslip with a random orientation^{6,7}. To create a physiologically relevant environment, it is important that such a model system recapitulate the 3D aspects of specific organs or tissues. More specifically, in our body, the cell bodies and dendrites of MNs are located in the spinal cord (CNS) to receive signals, whereas SCs and the axons of MNs are located in the PNS and form myelinated nerve fibers to deliver signals to the target muscle (Fig. 1a).

Correspondence: Dongeun Huh (huhd@seas.upenn.edu) or Seok Chung (sidchung@korea.ac.kr)

¹School of Mechanical Engineering, Korea University, 145 Anam-ro, Seongbuk-gu, Seoul 02841, South Korea

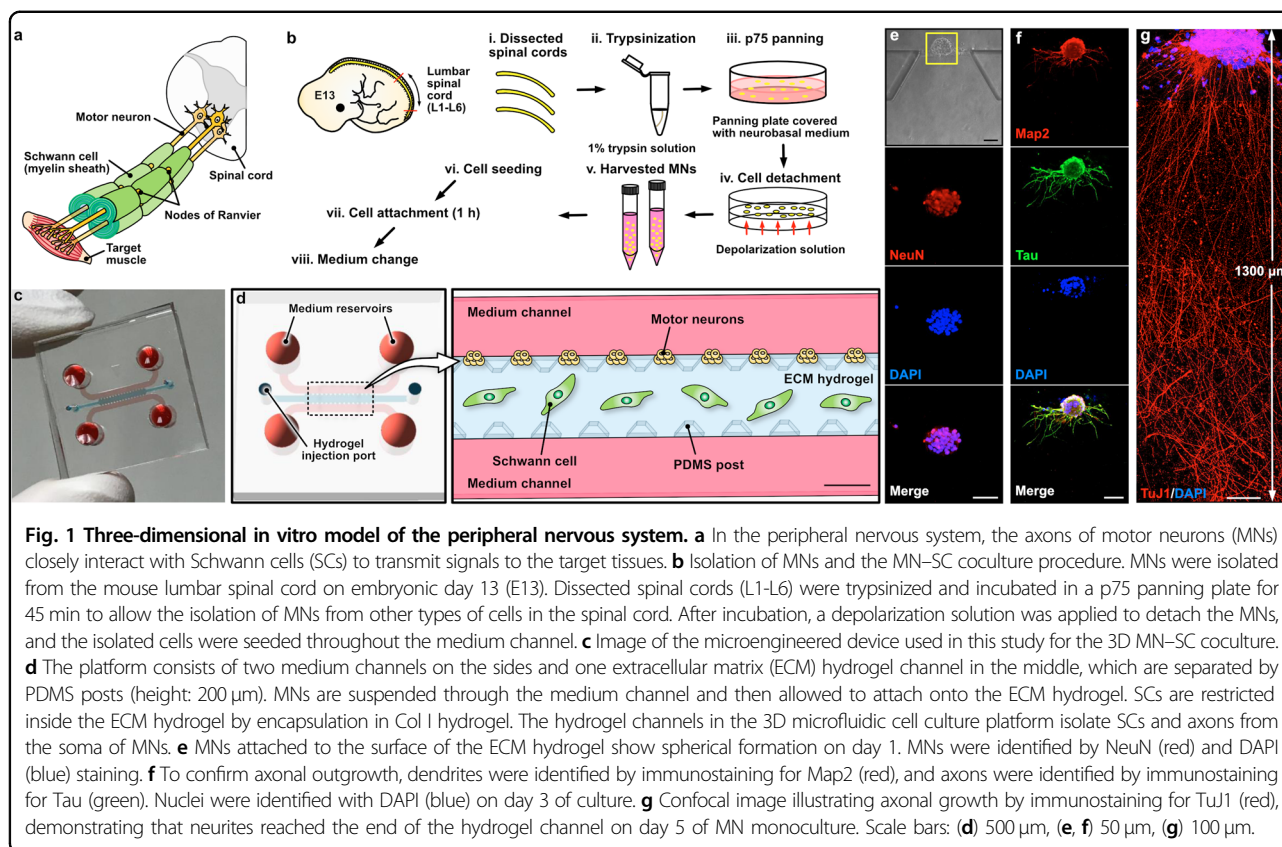
²Department of Bioengineering, University of Pennsylvania, Philadelphia, PA 19104, USA

Full list of author information is available at the end of the article

© The Author(s) 2021



Open Access This article is licensed under a Creative Commons Attribution 4.0 International License, which permits use, sharing, adaptation, distribution and reproduction in any medium or format, as long as you give appropriate credit to the original author(s) and the source, provide a link to the Creative Commons license, and indicate if changes were made. The images or other third party material in this article are included in the article's Creative Commons license, unless indicated otherwise in a credit line to the material. If material is not included in the article's Creative Commons license and your intended use is not permitted by statutory regulation or exceeds the permitted use, you will need to obtain permission directly from the copyright holder. To view a copy of this license, visit <http://creativecommons.org/licenses/by/4.0/>.



Recently, various microfabricated platforms have been developed to enable the coculture of spatially regulated cells at the cellular microenvironment scale^{8,9}. By taking advantage of microfabrication technology, it is possible to establish a PNS myelination model in a 3D microenvironment that would improve our ability to study motor neuron diseases in a more physiologically relevant context.

Here, we demonstrate the use of a microfabrication technique to develop a long-term cell culture platform that can be used for 3D compartmentalization of primary MNs and SCs. We describe the fabrication and assessment of a feasible 3D cell culture platform in which the SCs and MN axons are located within the extracellular matrix (ECM) hydrogel and the polarity of axonal outgrowth can be achieved with spatial separation from the MN cell bodies and dendrites. Using this microengineered ECM scaffold, we investigated the cellular behaviors of MNs and SCs in a 3D environment. Then, the effect of the MN–SC coculture on cell growth and maturation was studied. Our model was further developed into a peripheral myelination model by treating it with ascorbic acid (AA), which is known to regulate basal lamina and myelin formation by SCs by increasing the expression of myelin-related genes^{10,11}. To demonstrate the potential application in disease modeling, myelinated nerve fibers were treated with a high concentration of glial growth factor

(GGF, neuregulin-1 isoform) to block myelination and to produce a demyelination model¹². Taken together, our results indicate that our 3D in vitro PNS model has utility for the assessment of PNS myelination and demyelination by culturing MNs and SCs within the microengineered device. The model established in this study may have significant applications for motor neuron diseases by providing a drug screening platform for developing novel therapeutics.

Materials and methods

Fabrication of the silicon wafer and PDMS chip

The 3D microfluidic platform was fabricated based on the protocol described in our previous study⁸. Briefly, a cleaned and dehydrated 4-inch silicon wafer was spin-coated with SU-8 resist at a thickness of 200 µm with patterning and prebaked on a hot plate at 65 °C for 20 min and at 95 °C for 50 min (Supplementary Fig. 1). The coated wafer was exposed to UV light and postbaked on a hot plate at 65 °C for 1 min and at 95 °C for 12 min. The wafer was then developed in a photoresist developer for 15 min and finally rinsed with isopropyl alcohol (IPA) and dried with pressurized nitrogen gas. Polydimethylsiloxane (PDMS) devices were fabricated using soft lithography. Sylgard 184 silicone elastomer base (Dow Corning, USA) and the curing agent were combined at a ratio of 10:1

(w/w), mixed thoroughly, and poured over the master wafer at a thickness of 5 mm. Air bubbles were removed by degassing the wafer under a vacuum, and the PDMS was then allowed to polymerize in the oven for 24 h at 80 °C. The cured PDMS was removed from the wafer using a scalpel, and the holes through the reservoir patterns were created using a 4 mm disposable biopsy punch. For the hydrogel filling inlets, a 1 mm disposable biopsy punch was used. Small particles on the PDMS were removed using Scotch tape, and the PDMS was placed in a glass beaker filled with deionized (DI) water and sterilized using an autoclave. The devices were dry autoclaved once more by placing the PDMS in a clean box with the channel sides facing up. The sterilized devices were incubated in the oven for 24 h at 80 °C. Devices were then placed in plasma cleaner with glass coverslips, and the treated PDMS surface was bonded to the glass coverslip using sterile tweezers. The bonded devices were placed in the oven for 24 h at 80 °C and stored at room temperature until use.

Collagen gel preparation and filling procedure

To make the collagen gel solution, 20 μ L of 10X phosphate buffered saline (PBS) with phenol red was added into a sterile 1.5 mL tube (Supplementary Fig. 2). Then, 5 μ L of 0.5 N NaOH was carefully added into the same tube followed by 58.4 μ L of DI water. Finally, a total volume of 116.6 μ L of collagen type I, rat tail (Col I; BD Bioscience, cat. #40236) stock solution (stock concentration: 3.43 mg/mL) was added and carefully mixed until the gel appeared uniformly distributed. The final concentration of the Col I solution was set to 2 mg/mL, and the pH of the resultant solution was measured (pH 7.4). To fill the PDMS device with gel, a prewarmed humid chamber was prepared. The Col I gel solution was carefully injected into the hydrogel scaffold region using a 10 μ L micropipette. After gel filling, the devices were placed in a humid chamber with the channel side facing up. The humid chamber was then placed in a CO₂ incubator at 37 °C for 30 min to allow gelation. After incubation, the medium channels of the device were filled with the appropriate cell culture medium, and the device was placed in a CO₂ incubator until addition of the cell suspension.

Primary motor neuron culture

Motor neurons (MNs) were isolated from the lumbar spinal cord of CD-1 mice (E13) according to a previously described procedure¹³. Carefully, the lumbar region of the spinal cord (L1–L6 segment) was collected separately in a sterile 1.5 mL tube with 180 μ L of Hank's balanced salt solution (HBSS) on ice (Fig. 1b). Then, 20 μ L of a 1% trypsin solution (Worthington, USA) was added and carefully mixed. Trypsinization was performed by placing the tubes

in a 37 °C water bath for 15 min. After incubation, trypsinization was stopped by adding 20 μ L of 1% trypsin inhibitor (Sigma, USA), and gentle trituration was performed using a 200 μ L pipette tip. Cells were transferred to a prepared panning plate with a p75NTR antibody solution (1:5000; Abcam, UK) covered with GlutaMAX 1-containing (Gibco, USA) neurobasal medium (Gibco, USA). The panning plate was sealed with parafilm and incubated for 45 min at room temperature. The plate was washed three times with prewarmed neurobasal medium containing GlutaMAX 1, then with 300 μ L of depolarization solution containing 30 mM potassium chloride and 0.8% sodium chloride; and 2 mM calcium chloride was added after the last washing step to detach the cells from the panning plate. After 10 s, 500 μ L of prewarmed MN culture medium composed of neurobasal medium, 10% horse serum (HS; Gibco, USA), 1x GlutaMAX 1, 1x B27 supplement (Gibco, USA), 1 μ M β -mercaptoethanol (Sigma, USA), and 10 ng/mL BDNF (Gibco, USA) was added. Cells were collected in a sterile 15 mL tube by pipetting them up and down and then centrifuged at 400g for 5 min at room temperature. After centrifugation, the cells were resuspended in MN culture medium and seeded on the prepared device by adding 60 μ L of cell suspension into the reservoir at a density of 1×10^6 cells/mL. The devices were placed in an incubator containing CO₂ for 1 h to allow cell attachment, and the medium was replaced by adding 60 μ L of fresh MN culture medium to each reservoir.

Schwann cell culture

Mouse SCs were obtained from ScienCell Research Laboratories (#M1700; USA). SCs were maintained in basal medium supplemented with 5% fetal bovine serum (FBS), 1% SC growth supplement (SCGS), and 1% penicillin/streptomycin (P/S) solution.

Motor neuron–Schwann cell coculture

For the MN–SC coculture, mouse SCs were mixed in a Col I solution and seeded into the device through the hydrogel scaffold region at a density of 5×10^5 cells/mL 7 days prior to MN culture. SCs were cultured for 1 week with SC medium composed of basal medium (#1701; ScienCell, USA), 5% FBS (ScienCell, USA), 1% SCGS (ScienCell, USA), and 1% P/S solution. On day 0, MNs were seeded by adding 60 μ L of the cell suspension into the reservoir at a density of 1×10^6 cells/mL. Until day 7, MN–SC coculture medium composed of neurobasal medium, 10% HS, 0.5 mM L-glutamine (L-gln; Gibco, USA), 1x B27 supplement, 1 μ M β -mercaptoethanol, 0.5 μ M forskolin (Sigma, USA), 1 μ g/mL bovine pituitary extract (Thermo Fisher Scientific, USA), and 10 ng/mL BDNF was refreshed daily. After day 7, 50 μ g/mL ascorbic acid (AA; Sigma, USA) was added to the MN–SC coculture medium to induce myelination. To induce

demyelination, 200 ng/mL GGF (neuregulin-1 isoform) was added to the AA-supplemented MN–SC coculture medium starting on day 14.

Enzyme-linked immunosorbent assay

The concentrations of nerve growth factor (NGF) and glial cell-derived neurotrophic factor (GDNF) were measured using mouse NGF (CSB-E04684m; CUSABIO, USA) and GDNF (ab171178; Abcam, UK) enzyme-linked immunosorbent assay (ELISA) kits. Using these kits, the minimum levels of NGF and GDNF detection were 1.56 and 31.2 pg/mL, respectively. In brief, 100 μ L of standard or sample was added in duplicate, and the plate was incubated for 2 h at 37 °C. After incubation, the liquid in each well was removed, and 100 μ L of biotin antibody (1x) was added to each well. After 1 h of incubation at 37 °C, the plate was washed three times with 200 μ L of wash buffer, and 100 μ L of HRP-avidin (1x) was added to each well and incubated for 1 h at 37 °C. After washing 5 times, 90 μ L of TMB substrate was added to each well and incubated for 25 min at 37 °C protected from light. Then, 50 μ L of stop solution was added, and the optical density of NGF or GDNF was detected immediately at a 450 nm wavelength. The final concentration of NGF or GDNF was calculated according to the fitted standard curve.

Antibodies

The following antibodies were used in this study: mouse monoclonal anti- β 3-tubulin (TuJ1; ab78078, 1:1000), rabbit polyclonal anti-MAP2 (ab32454, 1:1000), rabbit polyclonal anti- β 3-tubulin (TuJ1; ab18207, 1:1000), mouse monoclonal anti-200 kD-neurofilament heavy (NF-H; ab7795, 1:1000), rabbit polyclonal anti-200 kD-neurofilament heavy (NF-H; ab8135, 1:1000), rabbit polyclonal anti-myelin basic protein (MBP; ab40390, 1:200), rabbit polyclonal anti-PMP22 (ab211052, 1:200), rabbit polyclonal anti-myelin protein zero (P0; ab31851, 1:100), rabbit polyclonal anti-Caspr (ab34151, 1:1000), rabbit monoclonal anti-S100 β (ab52642, 1:100), mouse monoclonal anti-Tau (ab80576, 1:200), mouse monoclonal anti-160 kD-neurofilament medium (NF-M; ab7794, 1:1000), goat anti-rabbit IgG H&L (TRITC; ab6718, 1:1000), goat anti-mouse IgG H&L (FITC; ab6785, 1:1000), and CytoPainter Phalloidin-iFluor 488 reagent (ab176753, 1:1000) from Abcam (UK).

Immunofluorescence assay

Cells cultured on microfluidic devices or coverslips were rinsed with phosphate-buffered saline (PBS) and fixed with 4% paraformaldehyde (PFA) for 15 min at room temperature. The fixed samples were washed twice with PBS, and 60 μ L of 0.1% Triton X-100 (Thermo Fisher Scientific, USA) was added to each reservoir for 3 min at room temperature. Then, the devices were washed twice

with PBS, and 60 μ L of 3% BSA (Sigma, USA) was added and incubated for 24 h at 4 °C. After washing the devices with PBS, the samples were incubated for 24 h at 4 °C with the primary antibodies. The devices were then washed twice with PBS and incubated with the secondary antibodies for 24 h at 4 °C. For nuclear staining, DAPI (D1306, 1:1000), which was obtained from Life Technologies (USA), was added to the secondary antibody solution. After washing the devices twice with PBS, all reservoirs were filled with 60 μ L of fresh PBS and placed on a shaker for 24 h at 4 °C. Confocal fluorescence images were captured on a confocal laser scanning microscope (LSM 700; Carl Zeiss, Germany) using a 20X/0.8 NA objective. Images were acquired by creating confocal z-stacks spanning from the minimum to the maximum depth of the ECM hydrogel region with 1 μ m intervals, each of which had a resolution of 1024 \times 1024. The obtained images were processed using ZEN 2011 (Zeiss, Germany) and ImageJ (National Institutes of Health, USA) with the projections of the z-stacks at the maximum intensity.

Transmission electron microscopy

Samples were fixed with 2.5% glutaraldehyde (Sigma, USA) in 0.1 M PBS (pH 7.4) for 24 h at 4 °C. After washing with 0.1 M PBS, the samples were postfixed with 1% osmium tetroxide (OsO₄) in 0.1 M sodium cacodylate trihydrate buffer for 1 h at room temperature. Then, the samples were dehydrated in a series of ethanol solutions (70%-80%-85%-90%-95%-100%-100%) followed by dehydration twice in pure propylene. Samples were embedded with the Epoxy Embedding Medium Kit (Sigma, USA). The silicone membranes were detached from the PDMS chip, and the embedded samples were removed from the microchannels. The samples were then cut into ultrathin sections (70–80 nm) using an ultramicrotome (Leica, Germany) and stained with uranyl acetate and lead citrate for transmission electron microscopy (TEM) imaging. Cryo-TEM (CryoTecnai F20; FEI, USA) was used to observe the samples.

Statistical analysis

For the statistical analysis, one-way analysis of variance (ANOVA) followed by Tukey's post hoc test was performed for the between-group comparisons, and the following *P* values were considered statistically significant: **P* < 0.05, ***P* < 0.01, and ****P* < 0.001. All data are expressed as the mean \pm standard error of the mean (SEM).

Results and discussion

Establishment of an in vitro peripheral nervous system model in a three-dimensional microenvironment

Our microengineered cell culture platform consists of two medium channels on the side and a hydrogel channel in the middle (Fig. 1c). The design of the device allows

SCs to be encapsulated in a Col I hydrogel separately from the cell bodies of MNs (Fig. 1d). In addition, the Col I gel in the hydrogel channel allows the axon but not the cell body to grow into the ECM hydrogel. It is important to note that this is an important feature of PNS myelination, and by mimicking this architecture, our device allows focused investigation of axon–SC interactions during the myelination process.

Prior to investigating the characteristics of MNs in our device, we used the neuron-specific marker NeuN to confirm the identify of MNs isolated from spinal cords (Fig. 1e). In addition, MAP2 (dendrites) and tau (axons) antibodies were used to measure the length of the neurites and evaluate dendritic and axonal outgrowth in MN monocultures. On day 1 of MN culture, the axons began to grow in the ECM hydrogel. On day 3 of the culture, the axons were observed to extend significantly into the ECM hydrogel, while the dendrites largely remained close to the cell bodies of MNs, as assessed by immunocytochemistry (Fig. 1f). On day 5, the neurites extended by 1300 μm and reached the end of the hydrogel channel (Fig. 1g). Collectively, these data suggest that primary MNs can be cultured in our device, where axons are able to grow longer than 1 mm in a 3D microenvironment.

The role of SCs in axonal outgrowth

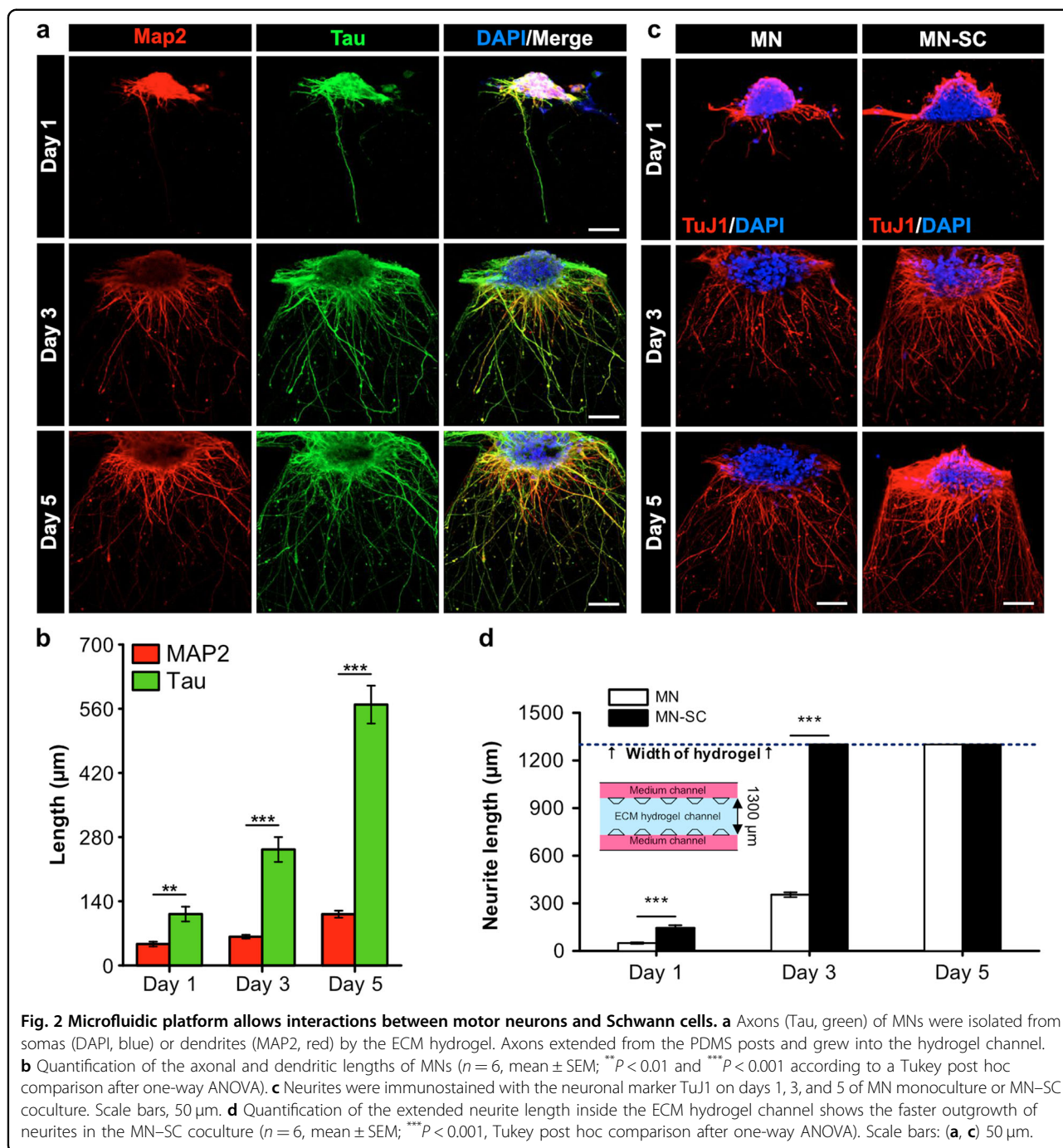
Next, we examined axonal outgrowth in the 3D microenvironment with and without SCs. Interestingly, significantly more axonal outgrowth was observed from day 1 of the MN monoculture compared to dendritic outgrowth (112.0 ± 16.0 and 46.6 ± 5.2 μm , respectively) (Fig. 2a, b). This tendency continued on days 3 and 5, as shown by the lengthening of axons (252.9 ± 27.0 and 569.2 ± 41.3 μm , respectively), whereas the majority of dendrites remained near the cell body of the MNs (65.6 ± 4.1 and 111.9 ± 7.8 μm , respectively) (Fig. 2a, b).

We then investigated the role of SCs in axonal outgrowth by comparing the MN monoculture and MN–SC coculture. Significant axonal outgrowth was observed starting on day 1 in the SC coculture, and axons reached the end of the hydrogel channel on day 3 (Fig. 2c). However, the relative axonal growth rate of the MN monoculture was slower than that of the MN–SC coculture. The mean neurite length on day 1 of the MN–SC coculture was 145 ± 16.5 μm , which was approximately three times longer than that of the MN monoculture (Fig. 2d). This difference was also observed on day 3 of culture, but the neurites reached the maximum length (width of the hydrogel channel, 1300 μm) by day 5 in both the MN–SC coculture and MN monoculture. These results support the role of SC in axonal outgrowth via the secretion of NGFs, which are crucial for establishing axonal regeneration and PNS regrowth following nerve injury¹⁴. Previous studies of

cells cultured on a 2D coverslip have reported that the axonal length in MN monocultures and MN–SC cocultures on day 2 was less than 50 and 150 μm , respectively, with an axonal growth rate of ~ 50 $\mu\text{m}/\text{day}$ ⁷. Thus, it is important to note that for MNs cultured in our platform, the axons grow five times faster than axons in cells cultured on 2D surfaces. Together, the results reveal that the 3D microenvironment and the presence of SCs accelerate axonal growth. However, it should be noted that the underlying mechanism of the chemical interactions between axons and SCs should be further investigated to provide a clear understanding of the role of SCs in axonal growth.

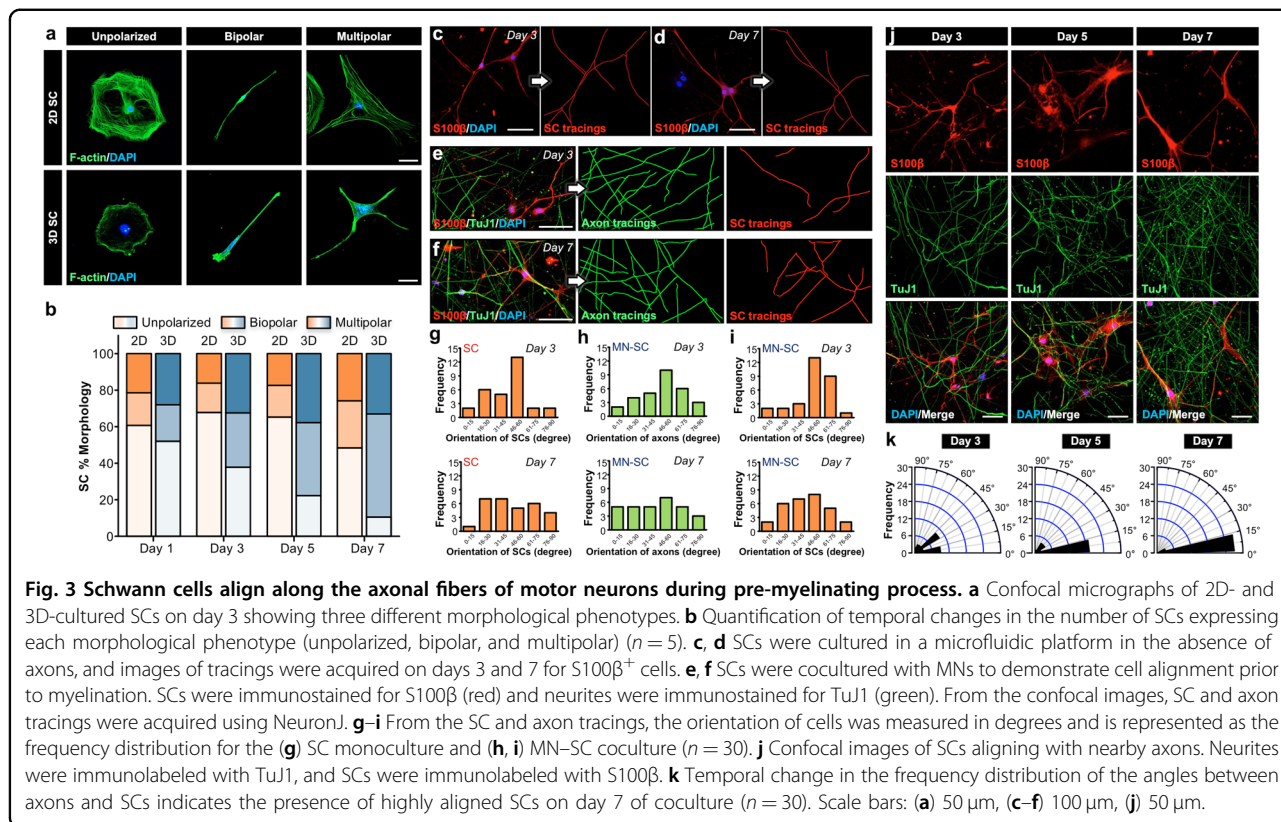
Morphological phenotype and alignment of Schwann cells in a 3D microenvironment

In vivo, SCs need to maintain their bipolar phenotypes to function in a biomechanical environment. However, when cultured in vitro, they exhibit motile phenotypes with three different forms: unpolarized, bipolar, and multipolar^{15,16}. We compared SCs cultured in the ECM hydrogel to those in 2D cultures to investigate the role of the 3D microenvironment in the phenotypic expression of SCs in the absence of MNs. First, mouse SCs were cultured on the microfluidic platform (3D) or a poly-D-lysine (PDL)-coated coverslip (2D) for 7 days (Fig. 3a). In both the 3D and 2D cultures, SCs displayed three morphological phenotypes when actin filament (F-actin) expression was visualized. The unpolarized phenotype showed a circular shape, with the nucleus located at the center of the SC. The bipolar and multipolar phenotypes were characterized by extensions (two for bipolar cells and three or more for multipolar cells) far from the nucleus. The different morphological phenotypes of SCs can undergo spontaneous transformation to different cell motility phenotypes during morphogenesis. To compare the percentages of the different cell motility phenotypes between the 3D and 2D in vitro cultures, the SC cytoskeleton was visualized with an F-actin antibody on days 1, 3, 5, and 7, and the number of cells displaying each phenotype was measured. The effect of the spatial environment on the SC phenotype was assessed by the percentage occurrence of each morphological phenotype in the 2D and 3D cell cultures (Fig. 3b). Three different morphological phenotypes of SCs were observed in vitro: unpolarized, bipolar, and multipolar. On the first day of 2D culture, SCs mainly displayed an unpolarized phenotype (60.7%), with 17.9% of cells displaying a bipolar phenotype. These percentages remained similar on day 7, with 48.4% of cells showing an unpolarized phenotype and 25.8% showing a bipolar phenotype. The percentage of each morphological phenotype in the 3D culture was similar to that in the 2D culture on day 1, with 52% of cells showing an unpolarized phenotype and 20% showing



a bipolar phenotype. However, on day 7, 56.5% of SCs displayed a bipolar phenotype, and 10.5% showed an unpolarized phenotype. Because the bipolar phenotype is known to be an important feature of motile and migratory SCs in the PNS¹⁵, our findings demonstrate that the Col I ECM-based scaffold created in our device played a critical role in providing a 3D environment that allows the spontaneous transformation of SCs into the bipolar phenotype, which is similar to that observed in vivo¹⁷.

We then examined the effect of axon–glial signaling on the morphological orientation of SCs. For the analysis, we immunostained SCs and MNs with S100 β and TuJ1 antibodies, respectively, and obtained their tracings using ImageJ (Fig. 3c–f). SCs were aligned with the proximal axons on day 7 of coculture; however, a random distribution of SC orientations was observed when SCs were cultured without MNs (Fig. 3g–i). Prior to initiating myelination, SCs migrate along outgrowing

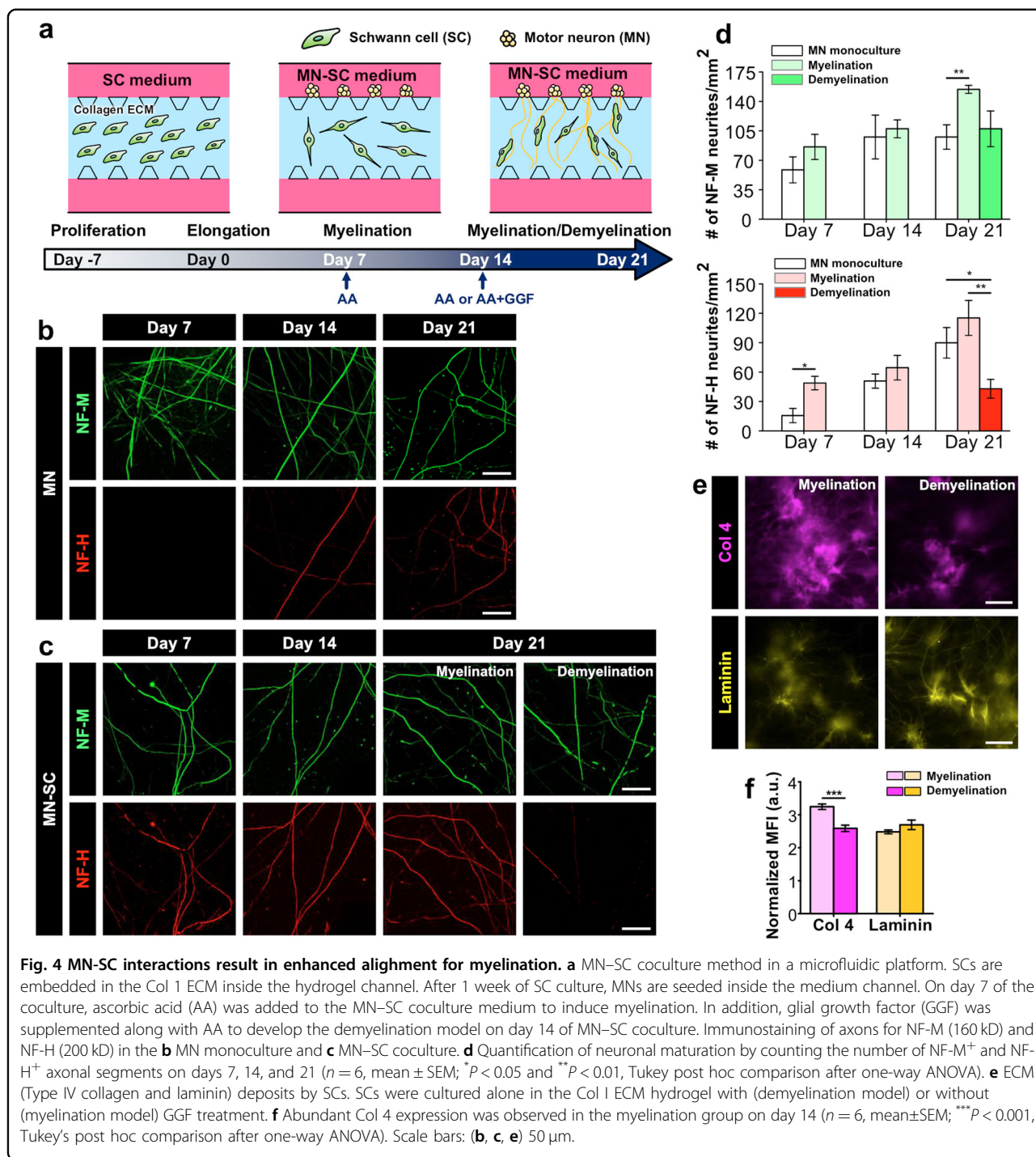


axons and communicate with them to provide a supportive environment for neurite outgrowth through the release of neurotrophic factors, expression of cell surface ligands, and synthesis of ECM (Fig. 3j)^{18–20}. The angle between the SC and the axons was measured to assess the alignment of the SC and adjacent axons (Fig. 3k). SCs cultured in the ECM hydrogel showed a random orientation on day 3 of the MN–SC coculture. However, on day 7, SCs closely associated with axons by aligning in the same direction via a physiological process similar to that which occurs *in vivo* during radial sorting^{21,22}. The angle (θ) measured between SCs and axons confirmed their alignment on days 5 and 7 of MN–SC coculture by exhibiting a high bias in the frequency distribution for $\theta < 15^\circ$. Our results suggest a tendency for SCs to migrate in the direction of proliferating axons prior to ensheathment, which also indicates that axon–SC interactions are associated with SC-induced directional neurite outgrowth and axonal-induced SC alignment^{23,24}.

Maturation of neurites in the myelination and demyelination models

We then investigated the effect of SCs on neuronal maturation by immunolabeling neurites with the NF-M (160 kD) and NF-H (200 kD) antibodies. During the MN–SC coculture, ascorbic acid (AA) was added starting

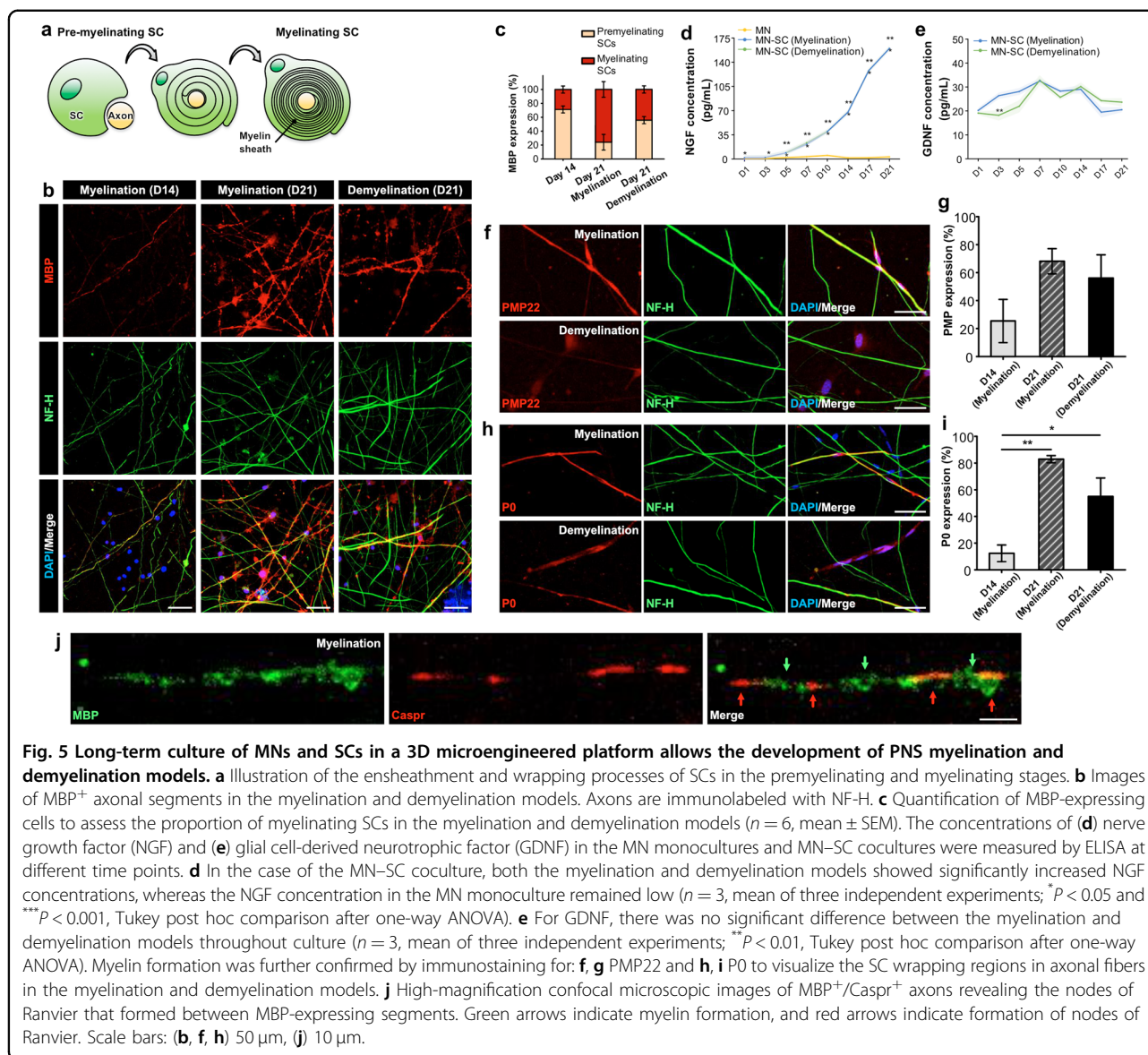
on day 7 to initiate myelination, and then GGF was added starting on day 14 to induce demyelination (Fig. 4a). In both the MN monoculture and MN–SC coculture, the mature neurites expressed both NF-M and NF-H (Fig. 4b, c). When the numbers of axons expressing NF-M and NF-H were counted, there was a significant difference in the number of NF-M⁺ neuronal segments on day 21 of culture (Fig. 4d). While there were 100.1 ± 18.4 neurites/mm² of NF-M⁺ axons in the MN monoculture, this number was significantly increased to 156.3 ± 9.8 neurites/mm² of NF-M⁺ axons in the MN–SC coculture model. In addition, a significant difference in the number of NF-H⁺ neurites between the MN monoculture and the MN–SC coculture was observed on day 7 (15.6 ± 7.3 and 48.8 ± 6.9 neurites/mm², respectively) (Fig. 4d). Furthermore, GGF treatment in the MN–SC coculture model significantly reduced the number of NF-H-expressing neurites on day 21. These results indicate that SC plays a critical role in neuronal maturation, as NF-H expression is low in developing neurons and increases in large, myelinated axons, and this tendency can be reversed in a demyelination model by GGF treatment. Furthermore, when treated with AA, the synthesis of collagen type 4 (Col 4) increased in the myelination model (Fig. 4e, f), supporting previous findings that showed Col 4 serves as a scaffold for the components of the basal lamina that attract SCs to attach to axons and initiate myelination^{10,25}.



Myelination and demyelination models of the PNS

In our device, supplementation of AA in the MN-SC coculture medium induced rapid myelin formation around the axonal segments, which was clearly visible in tubular structures in phase-contrast microscopy images obtained on days 14 and 21 (data not shown). We then further analyzed myelin formation by immunolabeling MBP. To quantify the proportion of SCs involved in

the myelination process, MBP⁺ cells were counted to determine the number of myelinating SCs (Fig. 5a). Terminally differentiated SCs forming compact myelin are known to express MBP^{26,27}, and MBP expression was detected in the MN-SC coculture model on days 14 and 21 (Fig. 5b). On day 14 of the MN-SC coculture, the SCs were mostly in the premyelinating stage, with only 28.7 \pm 5.0% of cells expressing MBP (Fig. 5c). However, a



higher percentage of SCs expressing MBP was observed on day 21 ($75.9 \pm 11.3\%$), indicating that the majority of SCs at this stage were in the myelinating process and had formed fully myelinated axonal segments. In contrast to the myelination model, GGF treatment in the demyelination model reduced the number of myelinating SCs on day 21 ($44.2 \pm 5.1\%$), indicating that maturation and myelination were suppressed in the demyelination model.

In the nervous system, glial cells are known to provide growth factors that support neuronal development^{28,29}. In our model, we previously found that SC plays an essential role in neuronal outgrowth and maturation. Specifically, when MNs were cultured with SCs, a significant increase in NGF was observed (Fig. 5d), which we believe promoted the

growth and stability of MNs throughout the culture period; however, this trend was not observed for GDNF (Fig. 5e).

In the PNS, fully mature myelinating SCs express peripheral myelin protein 22 (PMP22) and myelin protein zero (P0) when compact myelin is formed. PMP22 and P0 are known to regulate myelin formation, thickness and integrity^{30,31}. In the MN–SC coculture myelination model, abundant PMP22- and P0-expressing mature SCs along the axonal segments were clearly observed on day 21 when they were immunolabeled with NF-H, whereas the myelination process in cultures treated with GGF was blocked and showed decreased PMP22 and P0 expression (Fig. 5f–i). Thus, we demonstrated that supplementing AA in the MN–SC coculture medium allowed the maturation of SCs into myelinating cells to initiate wrapping and formation of

the myelin sheath, whereas GGF treatment of the MN–SC coculture inhibited this process.

Finally, formation of nodes of Ranvier in the myelination model were visualized by observing axonal organization in the perinodal regions using contactin-associated protein (Caspr) immunocytochemistry^{27,32–45}. On day 21 of the MN–SC coculture, Caspr-positive clusters were observed between the myelinated segments along the axons, representing formation of nodes of Ranvier (Fig. 5j). The presence of Caspr indicates that the nodes were mature in terms of their physiological morphologies, thus validating the in vitro myelination model in a 3D culture platform. The structure of the myelin sheath in our in vitro chip were further visualized using TEM cross-sectional images. In the MN monoculture, the presence of axons was observed throughout the culture (Supplementary Fig. 3). In the MN–SC coculture, unmyelinated axons with encapsulation of neurites by SCs were observed on day 7. On days 14 and 21, myelinating SCs were observed to be closely associated with axonal fibers (Supplementary Fig. 3). The presence of myelin sheaths was reduced in the MN–SC coculture group treated with GGF. Overall, our model showed both myelin formation and the development of nodes of Ranvier in ECM hydrogels and suggested that the cell culture setup in this study can serve as a tool to investigate the interaction between axons and SCs during myelination and demyelination.

Conclusion

An important aim of this study was to demonstrate an in vitro platform for MN–SC coculture to represent a model of the PNS and to assess the myelination process in a 3D environment. We proposed a robust method for modeling PNS myelination using a MN–SC coculture in a micro-engineered platform. This platform can be easily used to facilitate the coculture of different types of cells for bioengineering applications. Additionally, it can be used as a tool to assess axon–SC interactions during myelination and evaluate myelin formation in a more physiologically relevant environment than traditional 2D cell culture settings. In addition, we further showed the application of our model in disease modeling by demonstrating its capabilities to enable the long-term culture of MNs and SCs to expand scientific knowledge regarding the progressive stages of peripheral myelination, particularly in the study of motor neuron diseases.

Acknowledgements

This work was supported by the National Research Foundation (NRF) of Korea grant funded by the Korean government (MSIT) (No. 2017 M3C7A1028866) and the Korea Evaluation Institute of Industrial Technology (KEIT) grant funded by the Korean government (MSIT) (No. 20009125).

Author details

¹School of Mechanical Engineering, Korea University, 145 Anam-ro, Seongbuk-gu, Seoul 02841, South Korea. ²Department of Bioengineering, University of Pennsylvania, Philadelphia, PA 19104, USA. ³Biomedical Research Division, Korea Institute of Science and Technology, Hwarangno 14-gil 5, Seongbuk-gu, Seoul 02792, South Korea. ⁴NSF Science and Technology Center for

Engineering Mechanobiology, University of Pennsylvania, Philadelphia, PA 19104, USA. ⁵KHU-KIST Department of Converging Science and Technology, Kyung Hee University, 26, Kyungheedaero, Dongdaemun-gu, Seoul 02447, South Korea. ⁶Institute for Regenerative Medicine, Perelman School of Medicine, University of Pennsylvania, Philadelphia, PA 19104, USA. ⁷KU-KIST Graduate School of Converging Science and Technology, Korea University, 145 Anam-ro, Seongbuk-gu, Seoul 02841, South Korea

Conflict of interest

The authors declare that they have no conflict of interest.

Publisher's note

Springer Nature remains neutral with regard to jurisdictional claims in published maps and institutional affiliations.

Supplementary information is available for this paper at <https://doi.org/10.1038/s41427-020-00273-w>.

Received: 27 March 2020 Revised: 22 September 2020 Accepted: 1 October 2020.

Published online: 8 January 2021

References

- Garbay, B., Heape, A. M., Sargueil, F. & Cassagne, C. Myelin synthesis in the peripheral nervous system. *Prog. Neurobiol.* **61**, 267–304 (2000).
- Salzer, J. L. Schwann cell myelination. *Cold Spring Harb. Perspect. Biol.* **7**, 1–26 (2015).
- Jessen, K. R. & Mirsky, R. The origin and development of glial cells in peripheral nerves. *Nat. Rev. Neurosci.* **6**, 671–682 (2005).
- Salzer, J. L., Brophy, P. J. & Peles, E. Molecular domains of myelinated axons in the peripheral nervous system. *Glia* **56**, 1532–1540 (2008).
- Callizot, N., Combes, M., Steinschneider, R. & Poindron, P. A new long term in vitro model of myelination. *Exp. Cell Res.* **317**, 2374–2383 (2011).
- Stettner, M. et al. A reliable in vitro model for studying peripheral nerve myelination in mouse. *J. Neurosci. Methods* **214**, 69–79 (2013).
- Hyung, S. et al. Coculture of primary motor neurons and Schwann cells as a model for in vitro myelination. *Sci. Rep.* **5**, 15122 (2015).
- Shin, Y. et al. Microfluidic assay for simultaneous culture of multiple cell types on surfaces or within hydrogels. *Nat. Protoc.* **7**, 1247–1259 (2012).
- van Duinen, V., Trietsch, S. J., Joore, J., Vulto, P. & Hankemeier, T. Microfluidic 3D cell culture: from tools to tissue models. *Curr. Opin. Biotechnol.* **35**, 118–126 (2015).
- Eldridge, C. F., Bunge, M. B., Bunge, R. P. & Wood, P. M. Differentiation of axon-related Schwann cells in vitro. I. Ascorbic acid regulates basal lamina assembly and myelin formation. *J. Cell Biol.* **105**, 1023–1034 (1987).
- Laszkiewicz, I., Wiggins, R. C. & Konat, G. Ascorbic acid upregulates myelin gene expression in C6 glioma cells. *Metab. Brain Dis.* **7**, 157–164 (1992).
- Zanazzi, G. et al. Glial growth factor/neuregulin inhibits Schwann cell myelination and induces demyelination. *J. Cell Biol.* **152**, 1289–1299 (2001).
- Wiese, S. et al. Isolation and enrichment of embryonic mouse motoneurons from the lumbar spinal cord of individual mouse embryos. *Nat. Protoc.* **5**, 31–38 (2010).
- Toy, D. & Namgung, U. Role of glial cells in axonal regeneration. *Exp. Neurobiol.* **22**, 68–76 (2013).
- Mitchel, J. A. & Hoffman-Kim, D. Cellular scale anisotropic topography guides Schwann cell motility. *PLoS ONE* **6**, e24316 (2011).
- Lopez-Fagundo, C., Bar-Kochba, E., Livi, L. L., Hoffman-Kim, D. & Frank, C. Three-dimensional traction forces of Schwann cells on compliant substrates. *J. R. Soc. Interface* **11**, 20140247 (2014).
- Edmondson, R., Broglie, J. J., Adcock, A. F. & Yang, L. Three-dimensional cell culture systems and their applications in drug discovery and cell-based biosensors. *Assay. Drug Dev. Technol.* **12**, 207–218 (2014).
- Bunge, R. P. Tissue culture observations relevant to the study of axon–Schwann cell interactions during peripheral nerve development and repair. *J. Exp. Biol.* **132**, 21–34 (1987).

19. Fawcett, J. W. & Keynes, R. J. Peripheral nerve regeneration. *Annu. Rev. Neurosci.* **13**, 43–60 (1990).
20. Bunge, R. P. The role of the Schwann cell in trophic support and regeneration. *J. Neurol.* **242**, S19–S21 (1994).
21. Yoshimura, K. & Takeda, S. Hedgehog signaling regulates myelination in the peripheral nervous system through primary cilia. *Differentiation* **83**, S78–S85 (2012).
22. Feltri, M. L., Poitelon, Y. & Previtali, S. C. How Schwann cells sort axons: new concepts. *Neuroscientist* **22**, 252–265 (2016).
23. Thompson, D. M. & Buettner, H. M. Neurite outgrowth is directed by Schwann cell alignment in the absence of other guidance cues. *Ann. Biomed. Eng.* **34**, 669–676 (2006).
24. Heermann, S. & Schwab, M. H. Molecular control of Schwann cell migration along peripheral axons. *Cell Adhes. Migr.* **7**, 18–22 (2013).
25. Liazoghli, D., Roth, A. D., Thostrup, P. & Colman, D. R. Substrate micropatterning as a new in vitro cell culture system to study myelination. *ACS Chem. Neurosci.* **3**, 90–95 (2012).
26. Rumsey, J. W. et al. Node of Ranvier formation on motoneurons in vitro. *Biomaterials* **30**, 3567–3572 (2009).
27. Poliak, S. & Peles, E. The local differentiation of myelinated axons at nodes of Ranvier. *Nat. Rev. Neurosci.* **4**, 968–980 (2003).
28. Son, Y. J. & Thompson, W. J. Schwann cell processes guide regeneration of peripheral axons. *Neuron* **14**, 125–132 (1995).
29. Scheib, J. & Hoke, A. H. Advances in peripheral nerve regeneration. *Nat. Rev. Neurol.* **9**, 668–676 (2013).
30. Martini, R. & Schachner, M. Molecular bases of myelin formation as revealed by investigations on mice deficient in glial cell surface molecules. *Glia* **19**, 298–310 (1997).
31. Eichberg, J. Myelin P0: new knowledge and new roles. *Neurochem. Res.* **27**, 1331–1340 (2002).
32. Fex Svenningsen, A., Shan, W. S., Colman, D. R. & Pedraza, L. Rapid method for culturing embryonic neuron-glia cell cocultures. *J. Neurosci. Res.* **72**, 565–573 (2003).
33. Chan, J. R. et al. NGF controls axonal receptivity to myelination by Schwann cells or oligodendrocytes. *Neuron* **43**, 183–191 (2004).
34. Eshed, Y. et al. Gliomedin mediates Schwann cell-axon interaction and the molecular assembly of the nodes of Ranvier. *Neuron* **47**, 215–229 (2005).
35. Liu, N., Varma, S., Shooter, E. M. & Tolwani, R. J. Enhancement of Schwann cell myelin formation by K252a in the Trembler-J mouse dorsal root ganglion explant culture. *J. Neurosci. Res.* **79**, 310–317 (2005).
36. Honkanen, H. et al. Isolation, purification and expansion of myelination-competent, neonatal mouse Schwann cells. *Eur. J. Neurosci.* **26**, 953–964 (2007).
37. Gingras, M., Beaulieu, M. M., Gagnon, V., Durham, H. D. & Berthod, F. In vitro study of axonal migration and myelination of motor neurons in a three-dimensional tissue-engineered model. *Glia* **56**, 354–364 (2008).
38. Paivalainen, S. et al. Myelination in mouse dorsal root ganglion/Schwann cell cocultures. *Mol. Cell Neurosci.* **37**, 568–578 (2008).
39. Rangaraju, S., Madorsky, I., Pileggi, J. G., Kamal, A. & Notterpek, L. Pharmacological induction of the heat shock response improves myelination in a neuropathic model. *Neurobiol. Dis.* **32**, 105–115 (2008).
40. Feinberg, K. et al. A glial signal consisting of gliomedin and NrCAM clusters axonal Na⁺ channels during the formation of nodes of Ranvier. *Neuron* **65**, 490–502 (2010).
41. Susuki, K. et al. Schwann cell spectrins modulate peripheral nerve myelination. *Proc. Natl Acad. Sci. USA* **108**, 8009–8014 (2011).
42. Rumsey, J. W. et al. Myelination and node of Ranvier formation on sensory neurons in a defined in vitro system. *In Vitro Cell Dev. Biol. Anim.* **49**, 608–618 (2013).
43. Huval, R. M. et al. Microengineered peripheral nerve-on-a-chip for preclinical physiological testing. *Lab Chip* **15**, 2221–2232 (2015).
44. Sakai, K., Shimba, K., Kotani, K. & Jimbo, Y. A co-culture microtunnel technique demonstrating a significant contribution of unmyelinated Schwann cells to the acceleration of axonal conduction in Schwann cell-regulated peripheral nerve development. *Integr. Biol.* **9**, 678–686 (2017).
45. Khoshakhlagh, P., Sivakumar, A., Pace, L. A., Sazer, D. W. & Moore, M. J. Methods for fabrication and evaluation of a 3D microengineered model of myelinated peripheral nerve. *J. Neural Eng.* **15**, 064001 (2018).